https://doi.org/10.1007/s41230-020-0028-0

Effects of process parameters on semi-solid squeeze casting performance of aluminum alloy scrolls for scroll compressors

Yong-fei Wang[1, 2], Sheng-dun Zhao[1], *Yi Guo[3], Jun-ling Yang[4]

1. School of Mechanical Engineering, Xi'an Jiaotong University, Xi'an 710049, China

2. State Key Laboratory of Fluid Power and Mechatronic Systems, Zhejiang University, Hangzhou 310027, China,

3. School of Energy and Power Engineering, Xi'an Jiaotong University, Xi'an 710049, China

4. CAS Key Laboratory of Cryogenics, Technical Institute of Physics and Chemistry, Beijing 100190, China

Abstract: The aluminum alloy scroll is one of the key parts of the scroll compressors widely used in the air-conditioning, refrigeration, and heat pump systems. In this work, the semi-solid squeeze casting (SSSC) process was used to fabricate the aluminum alloy scroll. The effects of process parameters including the pouring temperature, mold temperature, and squeezing velocity on the filling and solidification behaviors of the alloys were investigated through simulations based on the power law cut-off (PLCO) material model. Results show that there is a significant increase in the flow velocity of the slurry, and the area of the high-speed region enlarges with the increase of the pouring temperature. The homogeneity of the temperature and velocity fields in the slurry is improved with an increase in mold temperature. Both the filling time and its variation rate decrease with an increase in squeezing velocity. The maximum solidification time exhibits a linear variation with the increase in pouring temperature. The shrinkage area is decreased by increasing the mold temperature. The optimal process parameters of the SSSC process were obtained from simulation analysis, which are the pouring temperature of 595 °C, mold temperature of 350 °C, and squeezing velocity of 0.3 $m \cdot s^{-1}$. Moreover, the qualified scroll casting was fabricated using the SSSC process under the optimal process parameters.

Key words: semi-solid squeeze casting; aluminum alloy; scroll compressor; numerical simulation; experimental verification

CLC numbers: TG146.21 **Document code:** A **Article ID:** 1672-6421(2020)05-347-10

Scroll compressors are widely used in air-conditioning, refrigeration, and heat pump systems [1] due to their advantages such as high volumetric efficiency, low vibration and noise, low torque variation, and low leakage [2]. They are also proposed to be applied in energy storage [3] and fuel cell systems [4] because of their excellent compression performance. A scroll compressor is a positive displacement machine which compresses the working fluid by two interfitting scrolls. The choice of manufacturing method is crucial for the scrolls due to the complex shape with involute curves [5]. The scroll for a typical refrigeration scroll compressor is generally fabricated by hot forging and machining processes. These manufacturing processes present certain disadvantages, such as a low material usage coefficient, low production efficiency, and high production cost [6-8]. Although the high pressure die casting can also be used for the fabrication of the scrolls, the gas and shrinkage porosity is inevitable due to the turbulent flow [9] resulting from the high filling rate [10].

Semi-solid metal forming (SSMF) is a promising process that can fabricate a near-net-shape forming part with high quality in one step [11-13]. Compared with conventional casting and forging, SSMF shows several potential advantages, such as reduced porosity [14], increased die life [15], less entrapped air [16], low forming force [17], and improved mechanical properties [18]. In addition, the squeeze casting (SC) process combines the advantages of die forging and die casting [19]. During the SC process, the molten metal is solidified under high pressure, which is favorable for obtaining excellent mechanical properties. Therefore, semi-solid squeeze casting (SSSC), which can be regarded

***Yi Guo**

Female, born in 1986, Ph.D., Associate Professor. Her research interests mainly focus on the design, manufacturing, semi-solid metal forming, and numerical simulation of the semi-solid squeeze casting process applied in the energy field.

E-mail: yiguo666@mail.xjtu.edu.cn

Received: 2020-03-10; Accepted: 2020-06-30

as a combination of SSMF and SC, can further improve the mechanical properties of products [20].

Studies on SC and SSSC have drawn significant attention from researchers in recent decades. Lee et al. [21] investigated the effects of melt temperature on melt flow and microstructure of squeeze cast B390 alloy scrolls. They reported that the sound orbiting scroll castings and the best melt filling patterns were obtained at 600 °C. Masoumi and Hu [22] studied the effects of the applied pressure on the tensile properties and microstructure of the SC AX51 alloy. Results showed that the fraction of the second phase and the porosity level decreased with the increase in the applied pressure, and therefore, the ultimate tensile strength, yield strength, and elongation increased. Ma et al. [23] established a pressure-driven mold filling model to predict the filling length of aluminum alloy melt/semi-solid slurry in the SSSC process. It was found that the proposed model was able to describe the filling behavior of aluminum alloys in the SSSC process with the corresponding rheological parameters and heat transfer coefficient. It was also found that a low pouring temperature would cause an incomplete filling, a high squeezing velocity would lead to a turbulent flow, and a low mold temperature would result in cold shut problems [24]. Therefore, it can be concluded that during SSSC, the process parameters have a significant impact on the product quality.

In this work, SSSC was proposed to fabricate the 2A50 alloy scrolls of the scroll compressor. The effects of process parameters including the pouring temperature, mold temperature and squeezing velocity on the slurry filling and solidification behaviors during the SSSC were investigated by using ProCast software with the power law cut-off (PLCO) material model. Moreover, the scrolls were fabricated with the optimal process parameters obtained from the simulation analysis.

1 Numerical methodology

1.1 Casting scheme and finite element model

The proposed casting scheme and the simulation model of the SSSC process for the scroll manufacture are shown in Fig. 1. There are four scrolls in one mold, as shown in Fig. 1(a), which consists of a vertical runner, four horizontal runners, four ingates, and twelve overflow troughs. One-fourth of the casting scheme is chosen as the computational domain in this study due to the symmetry, which is marked in the red dot-line square in Fig. 1(a). The tetrahedral grid is used for the mesh generation, as shown in Fig. 1(b). The grid independence calculation was carried out by using four sets of meshes including 79,287; 92,163; 103,083; and 113,285 grids. As shown in Table 1, the difference between the results of the maximum temperature drop under 103,083 and 113,285 grids was as low as 0.03%. Therefore, simulations were performed using the mesh with 103,083 grids.

The semi-solid 2A50 aluminum slurry was used as the material for fabricating the scroll. The thermal physical parameters of the alloy were obtained from the material library of ProCast software. Moreover, the PLCO model in ProCast

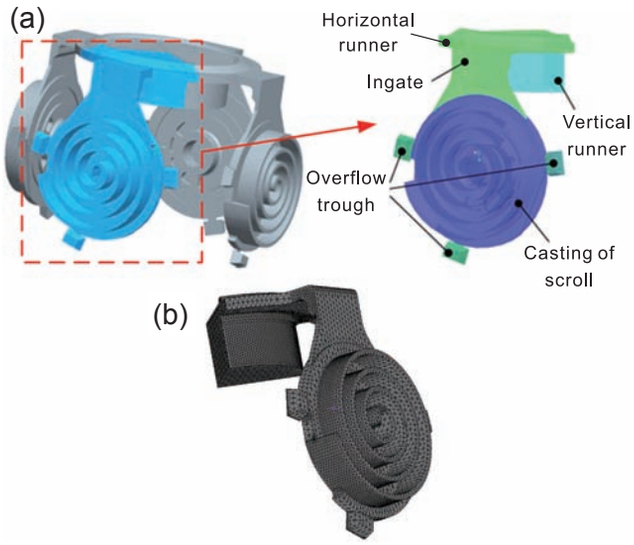

Fig. 1: Casting scheme (a) and mesh generation (b) of scroll and gating system by SSSC process

Table 1: Grid independence calculation

Mesh	Maximum temperature drop	
	Value (°C)	Relative error (%)
79,287	4.5256	6.8
92,163	4.3177	1.9
103,083	4.2394	0.03
113,285	4.2383	0.03

software was used to simulate the SSSC process for fabricating the scroll, where the material is assumed to be a viscous, isotropic, and incompressible fluid. The viscosity of the fluid in the PLCO model can be expressed by Eqs. (1) and (2) [25]:

$$\mu(\dot{\gamma}, T)=\mu_0(T)\,\dot{\gamma}_0^{n(T)} \quad \text{if } \dot{\gamma} \le \dot{\gamma}_0 \tag{1}$$

$$\mu(\dot{\gamma}, T)=\mu_0(T)\,\dot{\gamma}_0^{n(T)} \quad \text{if } \dot{\gamma} > \dot{\gamma}_0 \tag{2}$$

where μ is the dynamic viscosity, μ_0 is the temperature-dependent reference viscosity, $\dot{\gamma}$ is the local shear rate, $\dot{\gamma}_0$ is the cut-off shear rate and n is the shear thinning exponent. If $\dot{\gamma} > \dot{\gamma}_0$, the semisolid becomes more fluid, whereas if $\dot{\gamma} \le \dot{\gamma}_0$, its viscosity resumes to the value at the exit of the shot-sleeve [26].

1.2 Simulation settings of process parameters

Three process parameters including the pouring temperature, mold temperature and squeezing velocity significantly affect the filling ability of semi-solid slurry and the casting quality. To investigate the effect of process parameters, the simulation is conducted by varying the process parameters one by one while keeping the other two parameters invariant. Simulations can be classified into three groups, as shown in Table 2. The material of the mold in the simulation is set as H13 steel while the heat transfer coefficient between the mold and casting is set as 1,500 $W \cdot m^{-2} \cdot K^{-1}$.

Table 2: Input parameters in the simulation

Group No.	Pouring temperature (°C)	Mold temperature (°C)	Squeezing velocity (m·s^{-1})
A	580, 585, 590, 595, 600	400	0.5
B	600	200, 250, 300, 350	0.5
C	600	400	0.1, 0.2, 0.3, 0.4

2 Experimental

The experiments for manufacturing the scrolls were carried out by SSSC process under the optimized process parameters. Firstly, the 2A50 aluminum alloy was melted in a medium frequency induction furnace and maintained at 650±5 °C for 30 min. Secondly, the melt was poured into the stainless steel crucible, and EMS treatment was conducted with the AC of 30 A and the frequency of 30 Hz for 200 s, then the slurry, together with the crucible, was quenched with water to prepare the semi-solid billet. Thirdly, the semi-solid billet was remelted and held for 15 min to fabricate the scrolls by the SSSC process. The chemical composition of the 2A50 aluminum alloy is listed in Table 3. The solidus and liquidus temperatures of the 2A50 aluminum alloy are 521 °C and 615 °C, respectively. Moreover, the multi-directional squeeze casting mold, as shown in Fig. 2, was used.

Table 3: Chemical composition of the 2A50 aluminum alloy (wt. %)

Cu	Si	Mg	Mn	Zn	Ti	Ni	Fe	Al
2.43	0.82	0.68	0.53	0.12	0.06	0.05	0.01	Bal.

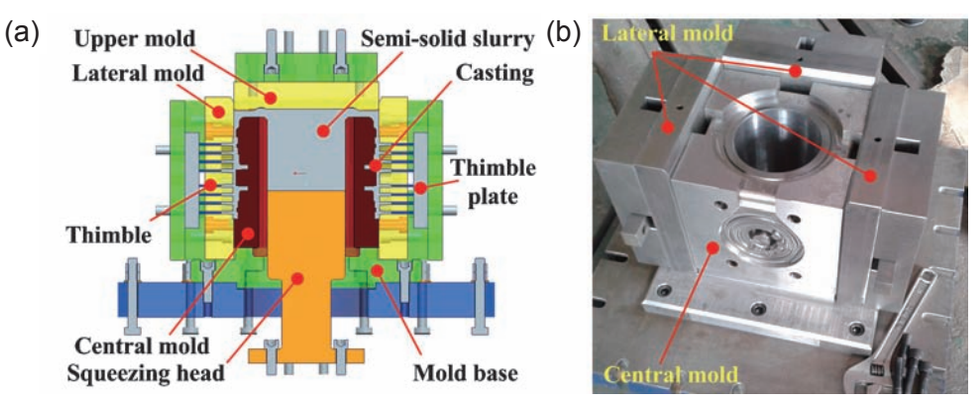

Fig. 2: Schematic (a) and experimental setup (b) of the multi-directional squeeze casting mold of the scroll

3 Results and discussion

3.1 Effects of pouring temperature on filling behavior

Figure 3 shows the temperature distributions of the slurry at pouring temperatures of 580, 590, and 600 °C under the squeezing velocity of 0.5 m·s^{-1} and a mold temperature of 400 °C. Although there is no significant variation of temperature at different regions of the slurry at each pouring temperature, a slight temperature drop is observed at the left and right side of the scroll during the filling process. The relatively low-temperature region at the pouring temperature of 590 °C is smaller than those at 580 and 600 °C.

The flow velocity distributions of the slurry at different pouring temperatures are presented in Fig. 4. The flow velocity of the slurry significantly increases with increasing of the pouring temperature. The area of the high-speed region is enlarged when the pouring temperature is increased. At the pouring temperature of 580 °C, the flow velocity of the slurry is generally below 0.6 m·s^{-1} with the velocity above 2.0 m·s^{-1} only at the inner runner and the central part due to the relatively low viscosity. Most flow velocities of the slurry are found above 3.2 m·s^{-1} when the pouring temperature is 590 °C. However, the velocity of the slurry at the bottom region is relatively low due to the thin wall and early filling in this location. When the pouring temperature is 600 °C, the high-speed area is almost as large as the entire scroll with the velocity of around 5.6 m·s^{-1}, except the right bottom region because of the low viscosity of the slurry. The results indicated that the pouring temperature of the slurry determined the initial viscosity of the slurry during the filling process, which in turn affected the fluidity of the slurry and changed the distribution characteristic of the velocity field.

The comparison of the maximum temperature drop of the slurry and average velocity in the ingate between different pouring temperatures is illustrated in Fig. 5. The maximum temperature drops of the slurry at the end of the filling procedure are all around 4.5 °C with a slight decrease with the increase of pouring temperature. The average velocity

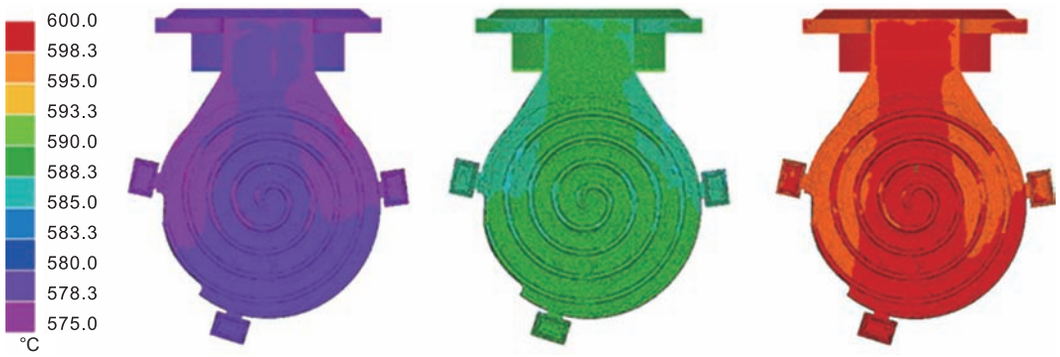

Fig. 3: Temperature distribution of the slurry at pouring temperatures of 580 °C (a), 590 °C (b), and 600 °C (c) (squeezing velocity: 0.5 m·s^{-1}, mold temperature: 400 °C)

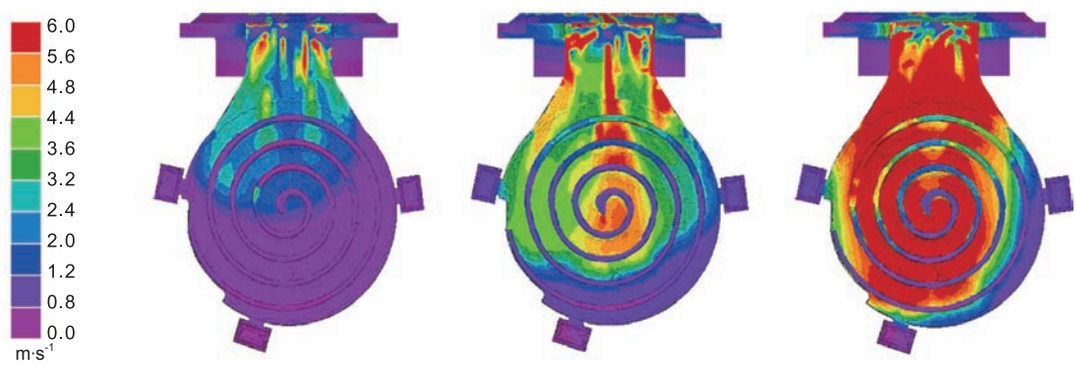

Fig. 4: Flow velocity distribution of slurry at pouring temperatures of 580 °C (a), 590 °C (b), and 600 °C (c) (squeezing velocity: 0.5 m·s^{-1}, mold temperature: 400 °C)

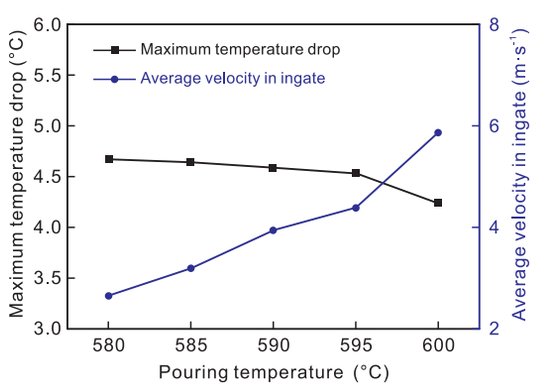

Fig. 5: Effects of pouring temperature on maximum temperature drop of slurry and average velocity in ingate

in the ingate linearly increases with the increase in pouring temperature due to the lower viscosity at a higher temperature. The increase ratio of the average velocity from 595 to 600 °C is the highest compared to other temperature differences. However, a high slurry velocity may introduce the turbulence flow, which would decrease the stability of the filling process and result in a decrease in product quality.

3.2 Effects of mold temperature on filling behavior

Figure 6 shows the temperature distribution of the slurry at mold temperatures of 200, 300, and 400 °C with the squeezing velocity of 0.5 m·s^{-1} and pouring temperature of 600 °C. The overall temperature of the slurry increases with the increase in the mold temperature. At all mold temperature conditions, the low-temperature field (marked with the black dotted line in Fig. 6) was observed at the top side area of the scroll. The homogeneity of the temperature was improved with the increase of the mold temperature. This is because a high mold temperature results in a low difference in the temperature between the mold and slurry, which consequently reduces the heat loss during the filling process.

The flow velocity distribution of the slurry at different mold temperatures is shown in Fig. 7. The largest low-velocity field (marked with the black dotted line in Fig. 7) is observed in the case of 200 °C at the bottom part of the scroll, which accounts for approximately one-third of the total area. It is noteworthy that the smallest area of the low-velocity field is found at the mold temperature of 300 °C instead of 400 °C, although the high-velocity field accounts for the largest proportion of the area when the temperature was 400 °C. However, the high-velocity region in the case of 400 °C reaches almost 80% of the total area, which leads to a more homogeneous velocity field under this mold temperature condition. This means that the increase in the mold temperature is beneficial for a homogeneous flow field in the filling process.

A summary of the maximum temperature drop of the slurry and the average velocity in the ingate under different mold temperatures is shown in Fig. 8. The maximum temperature

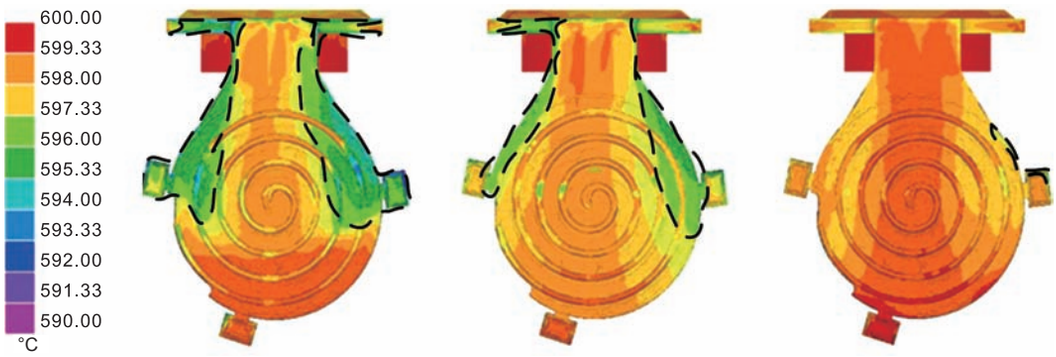

Fig. 6: Temperature distribution of slurry at mold temperatures of 200 °C (a), 300 °C (b), 400 °C (c) (squeezing velocity: 0.5 m·s^{-1}, pouring temperature: 600 °C)

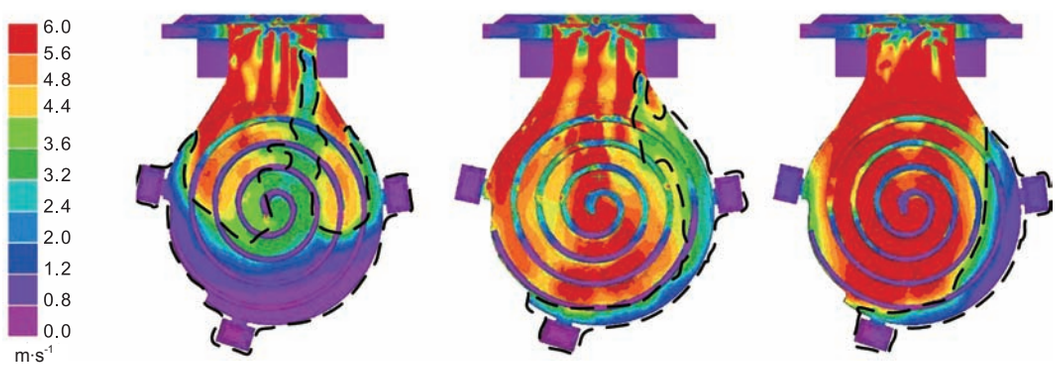

Fig. 7: Flow velocity distribution of the slurry at mold temperatures of 200 °C (a), 300 °C (b), 400 °C (c) (squeezing velocity: 0.5 m·s^{-1}, pouring temperature: 600 °C)

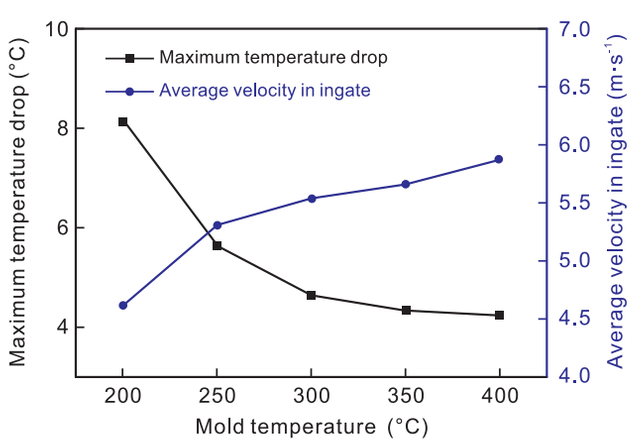

Fig. 8: Effects of mold temperature on the maximum temperature drop of the slurry and average velocity in ingate

drop is 8 °C when the mold temperature is 200 °C, which decreases with the increase in the mold temperature and tends to be stable at 4.24 °C when the mold temperature is higher than 300 °C. The average velocity in the ingate shows growth with the increase of the mold temperature from about 4.6 m·s^{-1} to around 5.9 m·s^{-1}. This was because a high temperature difference between slurry and mold leads to the reduction of heat loss, temperature drop, and viscosity, which consequently causes a high slurry velocity.

3.3 Effects of squeezing velocity on filling behavior

The temperature distribution of slurry at the squeezing velocity of 0.1, 0.3, and 0.5 m·s^{-1}, under the pouring temperature of 600 °C and a mold temperature of 400 °C is shown in Fig. 9. The overall temperature of the slurry was greater at a higher squeezing velocity due to the reduced time for heat exchange at a high velocity. The increase in the squeezing velocity improved the homogeneity of the temperature field of the slurry for the filling process. The most homogeneous temperature field was obtained at the squeezing velocity of 0.5 m·s^{-1}, while the most unhomogeneous was observed at 0.1 m·s^{-1}. The low-temperature field was found at the left and right side of the scroll at all squeezing velocities due to the enhanced heat exchange through the thin wall.

Figure 10 presents the velocity distribution of the slurry at different squeezing velocities. The average velocity of the slurry increases with the increase of the squeezing velocity. The distribution pattern of the velocity varies with the change in the squeezing velocity. When the squeeze velocity was 0.1 m·s^{-1}, the high-velocity field was found at the left and right side of the scroll, accounting for around half of the total area. The velocity at this high-velocity field was observed around 2.4 m·s^{-1}. At the squeeze velocity of 0.3 m·s^{-1}, the high-velocity field occupied the center and top regions of the scroll with the velocity of about 1.2 m·s^{-1}, accounting for approximately three-quarters of the whole filling area. When the squeeze velocity reached 0.5 m·s^{-1}, the velocity of the slurry in the high-velocity field increased up to 5.6 m·s^{-1}, which

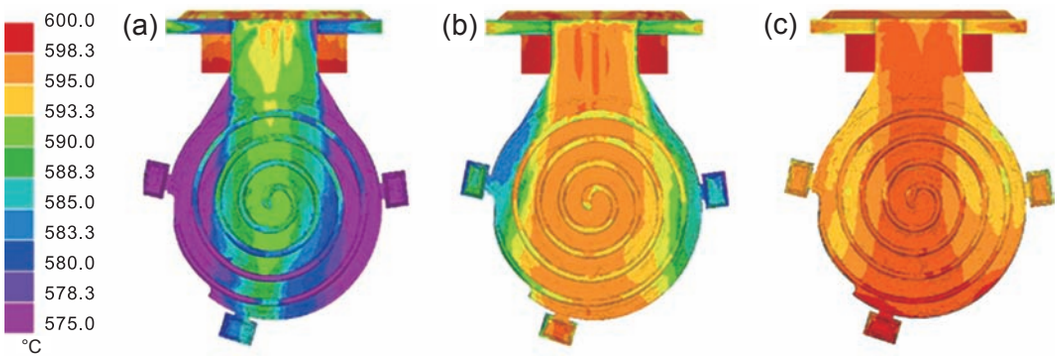

Fig. 9: Temperature distribution of slurry at squeezing velocities of 0.1 m·s^{-1} (a), 0.3 m·s^{-1} (b), 0.5 m·s^{-1} (c) (pouring temperature: 600 °C, mold temperature: 400 °C)

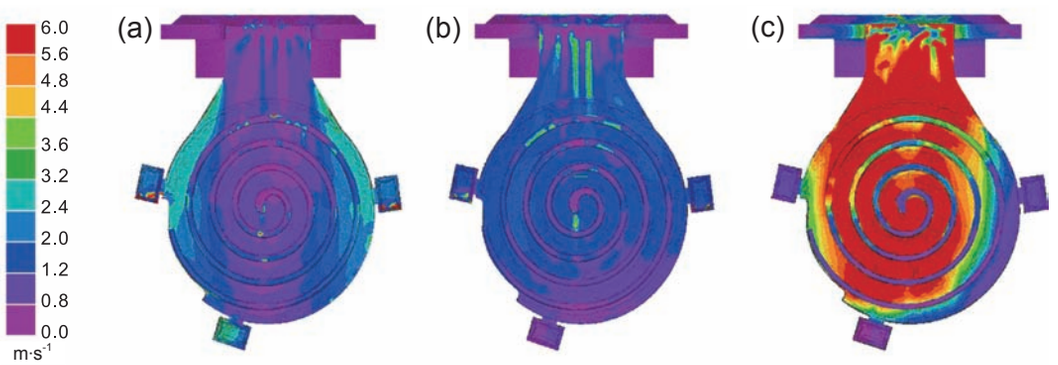

Fig. 10: Velocity distribution of slurry at squeezing velocities of 0.1 m·s^{-1} (a), 0.3 m·s^{-1} (b), 0.5 m·s^{-1} (c) (pouring temperature: 600 °C, mold temperature: 400 °C)

accounted for almost nine-tenths of the whole area with a small low-velocity region at the bottom right. Comparing Figs. 10(a) to (c), the most homogeneous velocity field was observed at the squeezing velocity of 0.3 m·s^{-1}.

Effects of squeezing velocity on the maximum temperature drop, the average velocity in the ingate and the required time of the filling procedure are illustrated in Fig. 11. As shown in Fig. 11(a), the maximum temperature drop decreases with an increase in squeezing velocity, indicating that high squeezing velocity can improve the homogeneity of temperature distribution. The average velocity in the ingate increased from 0.8 to 5.9 m·s^{-1} when the squeezing velocity varied from 0.1 to 0.5 m·s^{-1}, where it showed a linear increase from 0.1 to 0.4 m·s^{-1} and a significant increase at 0.5 m·s^{-1}. This is because the shearing speed rapidly increased with the increase in the squeezing velocity, leading to a rapid reduction of viscosity [27]. This decreased viscosity would cause the turbulence flow and reduce the flow stability of the filling process, which rapidly increase the average velocity in the ingate. As shown in Fig. 11, the filling time decreased from 1.25 to 0.3 s when the squeezing velocity increased from 0.1 to 0.5 m·s^{-1}. It can be seen that the variation speed of the filling time reduced with the increase in the squeezing velocity. At the squeezing velocity of 0.2 m·s^{-1}, it needed 0.66 s to finish the filling process, accounting for 52.8% of the time at the velocity of 0.1 m·s^{-1}. Furthermore, the filling time was only 0.36 s at the squeezing velocity of 0.4 m·s^{-1}, which was 28.8% of the time required at the velocity of 0.1 m·s^{-1}.

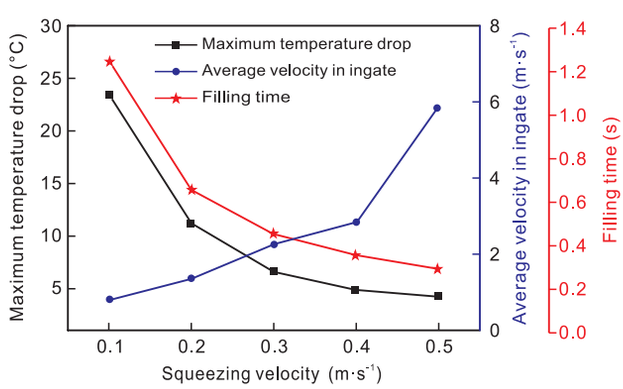

Fig. 11: Effects of squeezing velocity on maximum temperature drop of slurry and average velocity in ingate as well as filling time

3.4 Effects of pouring temperature on solidification behavior

The solidification time distribution and the maximum solidification time of the casting under different pouring temperatures are illustrated in Fig. 12. It is shown that the castings were solidified from the outer circular region of the scroll to the central part. The solidification time of the runner was relatively long due to the relatively large wall thickness. The feeding channel was solidified before the main body of the scroll casting. At the pouring temperature of 580 °C, most parts of the scroll casting were solidified within 16 s, while it

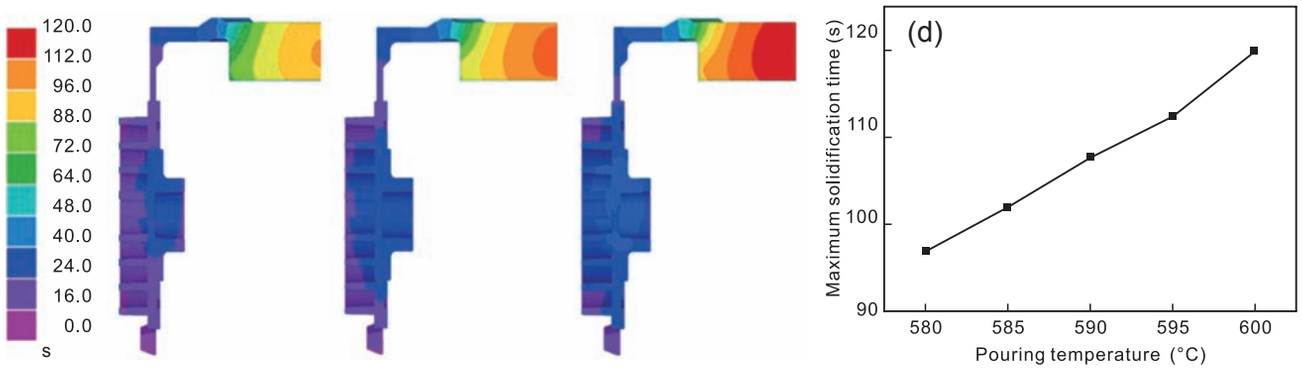

Fig. 12: Solidification time distribution under pouring temperatures of 580 °C (a), 590 °C (b), and 600 °C (c), and its changing trend with pouring temperature (d)

required 24 s at the pouring temperature of 600 °C. It can be seen in Fig. 12(d) that the maximum solidification time was observed as a linear variation with an increase in pouring temperature. A long solidification time would reduce the quality of the casting due to the coarsen of grains, which should be avoided for the manufacture of the scroll casting.

Figure 13 shows the temperature distribution of the casting at the solidification time of 8 s under the pouring temperatures of 580, 590, and 600 °C. It can be seen that the overall temperature of the casting increased with the increase in the pouring temperature. The temperature distribution patterns of the casting were similar to each other at different pouring temperatures. The temperature at the center of the casting and runner is significantly higher than the outer circular region. In the ingate, the temperature of the casting at the side region was lower than the center part, which means it solidified from the sides to the center in this location.

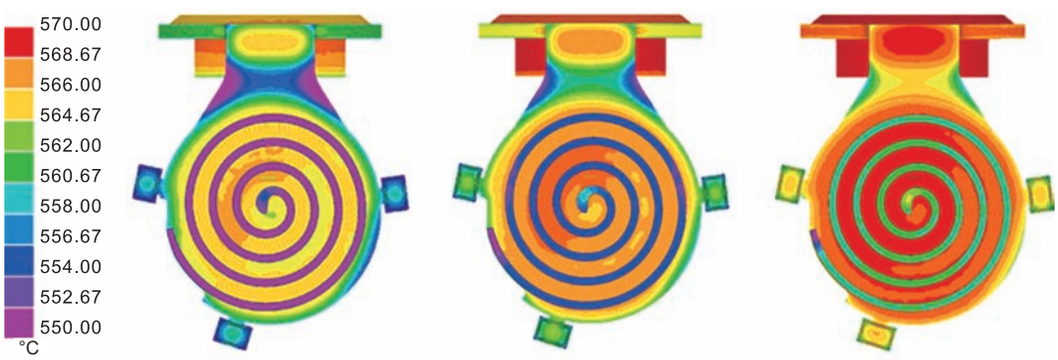

Fig. 13: Temperature distribution of the casting at pouring temperatures of 580 °C (a), 590 °C (b), and 600 °C (c) (squeezing velocity: 0.5 m·s^{-1}, mold temperature: 400 °C, solidification time: 8 s)

The variation of the shrinkage of the scroll casting at different pouring temperatures is presented in Fig. 14. The shrinkage area increased with the increase in pouring temperature. It can be seen that there was no shrinkage when the pouring temperature was 580 °C, while the shrinkage region was observed at 590 °C, and relatively large at 600 °C. This enlarged shrinkage region with increasing of the pouring temperature was resulted from the faster solidification of the feeding channel compared to the main body of the scroll casting, as shown in Fig. 12.

3.5 Effects of mold temperature on solidification behavior

The comparison of the solidification time distribution and the maximum solidification time between different mold temperatures is shown in Fig. 15. At the mold temperature of 200 °C, most parts of the scroll casting were solidified within 16 s. The solidification time was prolonged with the increase in the mold temperature, which increased from 55 s at the mold temperature of 200 °C to 120 s at the mold temperature of 400 °C. It showed a quadratic dependence of the maximum solidification time on mold temperature. The solid grain of the casting would further grow under the high temperature during a long solidification time, which negatively affects the mechanical properties of the casting. Therefore, the mold temperature should be appropriately chosen to reduce the solidification time and consequently reduce the shrinkage of the casting.

Figure 16 shows the temperature distribution of the casting at mold temperatures of 200, 300, and 400 °C, under the squeezing velocity of 0.5 m·s^{-1} and pouring temperature of 600 °C, with the solidification time of 8 s. The patterns of temperature distributions under different mold temperatures were similar to each other, where the temperature at the center of the casting

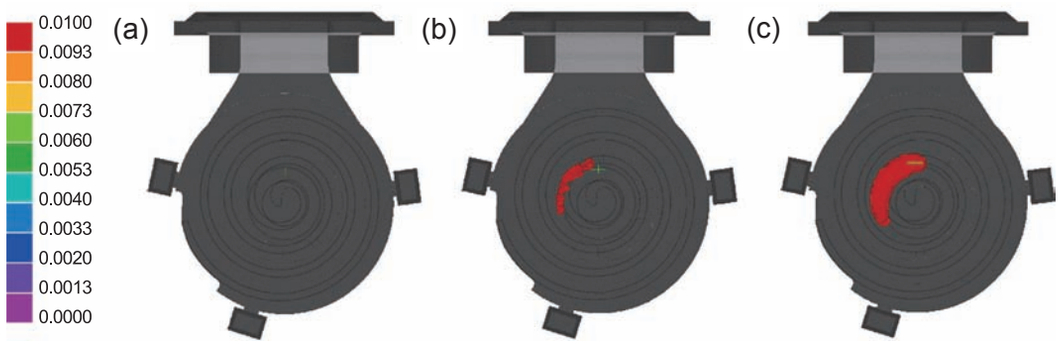

Fig. 14: Shrinkage distribution at pouring temperatures of 580 (a), 590 (b), 600 °C (c) (squeezing velocity: 0.5 m·s^{-1}, mold temperature: 400 °C, solidification time: 8 s)

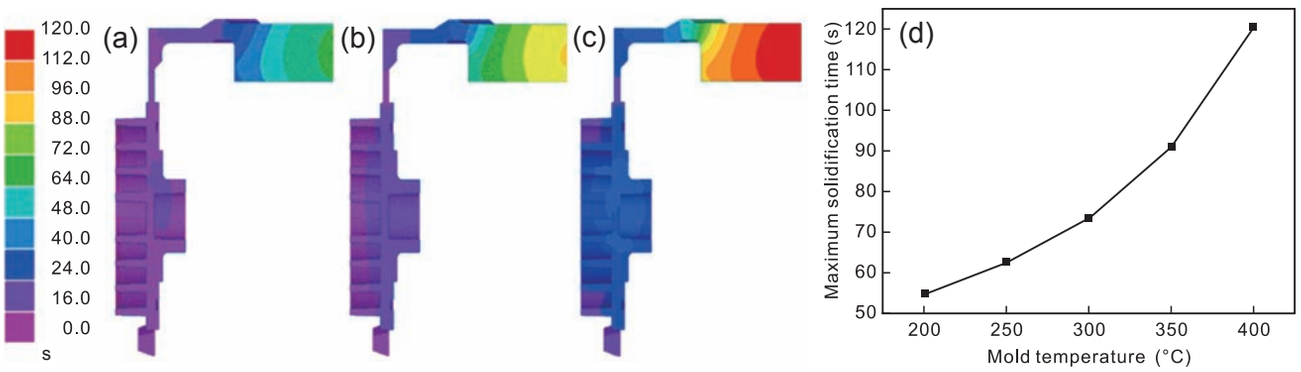

Fig. 15: Solidification time distribution under mold temperatures of 200 °C (a), 300 °C (b), and 400 °C (c), and the maximum solidification time at different mold temperatures (d)

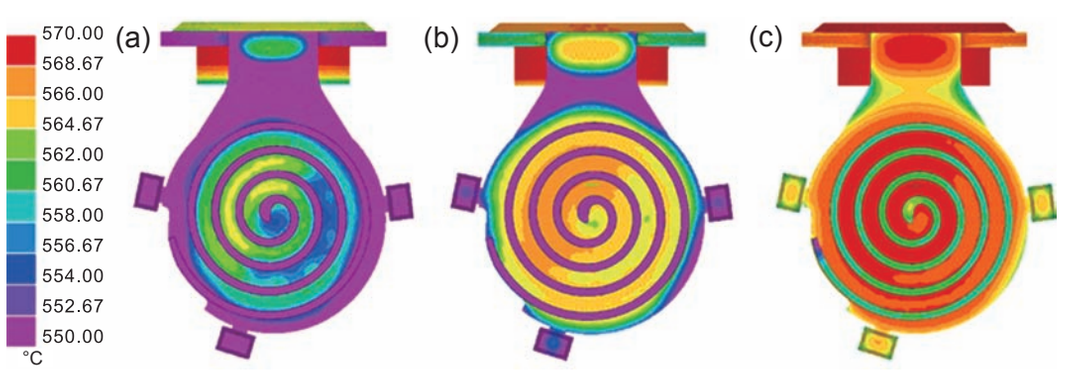

Fig. 16: Temperature distribution of casting at mold temperatures of 200 °C (a), 300 °C (b), and 400 °C (c) (squeezing velocity: 0.5 m·s^{-1}, pouring temperature: 600 °C, solidification time: 8 s)

and the vertical runner were significantly higher compared to the other regions. The temperature of the casting increased with the increase in mold temperature. The homogeneity of temperature distribution was also improved when the mold temperature was increased. Comparison of Fig. 13 with Fig. 16 showed that the effect of mold temperature on the temperature distribution was larger than the pouring temperature.

The distributions of the shrinkage area at different mold temperatures are shown in Fig. 17. The shrinkage area decreased when the mold temperature increased. This was because the slurry in the ingate solidified quickly due to the thin wall and the low mold temperature, which blocked the feeding of the slurry for the central part of the scroll. At the mold temperature of 200 °C, the shrinkage area occupied almost eight-tenths of the whole scroll, which decreased to around one-tenth of the casting at the temperature of 300 °C. The solidification time at the ingate enlarged when the mold temperature increased, which provided more time for feeding the slurry to the central part in the extra space generated by the cooling shrinkage.

3.6 Optimal process parameters for the semi-solid squeeze casting of aluminum alloy scrolls

According to the results in Sections 3.1 and 3.4, it can be concluded that the increase in the pouring temperature improved the homogeneity of the velocity field in the filling procedure. However, too high a pouring temperature increases the shrinkage area in the casting scroll. Therefore, the pouring

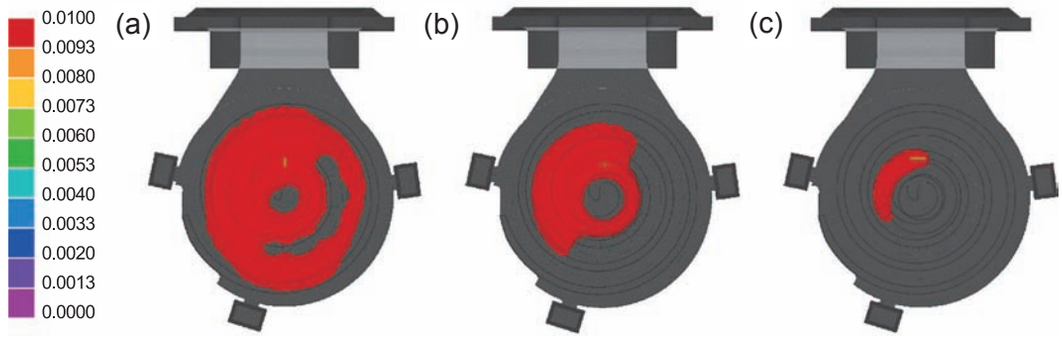

Fig. 17: Shrinkage distribution of the casting at mold temperatures of 200 °C (a), 300 °C (b), and 400 °C (c) (squeezing velocity: 0.5 m·s^{-1}; pouring temperature: 600 °C; solidification time: 8 s)

temperature of 595 °C is recommended for the SSSC process in this study. Findings from Sections 3.2 and 3.5 revealed that the increase in the mold temperature was able to improve the homogeneity of the velocity field in the filling procedure. The increase in the mold temperature can also decrease the shrinkage area of the casting scroll. Nevertheless, it showed a quadratic dependence of the maximum solidification time on mold temperature. As a long solidification time would cause a large grain size, the mold temperature of 350 °C is then recommended for the SSSC process. The recommended squeezing velocity is 0.3 m·s^{-1} as the most homogeneous velocity field was observed at this velocity as mentioned in Section 3.3.

The scroll casting by the SSSC process under the recommended process parameters is shown in Fig. 18, and the X-ray detection results of the scroll casting are shown in Fig. 19. It can be seen in Fig. 18 that the scroll casting produced by the SSSC process was fully filled. The profile of the scroll was clear, and the surface of the scroll was smooth. No obvious macroscopic defects such as shrinkage porosity, air entrapment, and cracks were observed. It can be concluded from Fig. 19 that a dense interior structure was obtained for the scroll casting and no obvious internal defects such as inclusions, bubbles or cold shut were observed. This means that the semi-solid slurry experienced qualified filling and solidification procedures under the recommended process parameters.

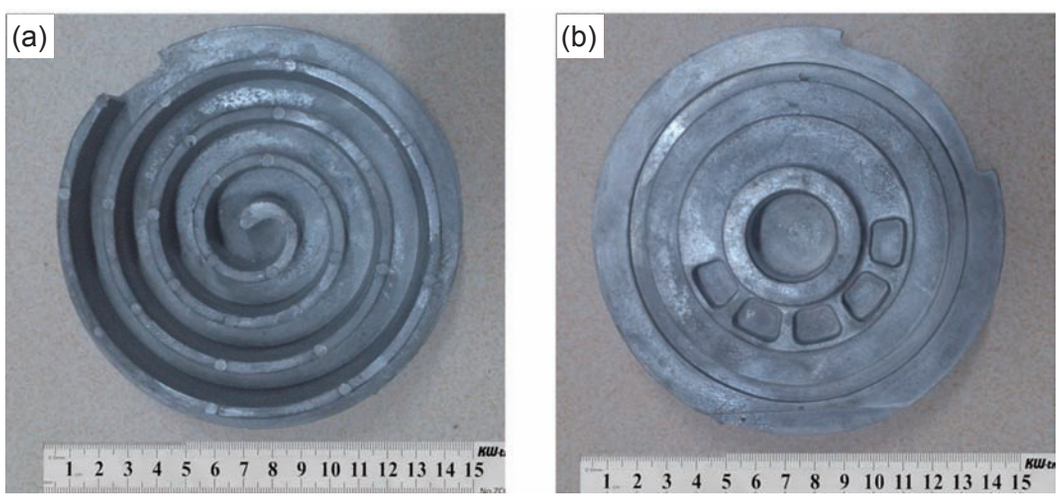

Fig. 18: Front view (a) and back view (b) of the scroll casting formed by SSSC process under recommended process parameters

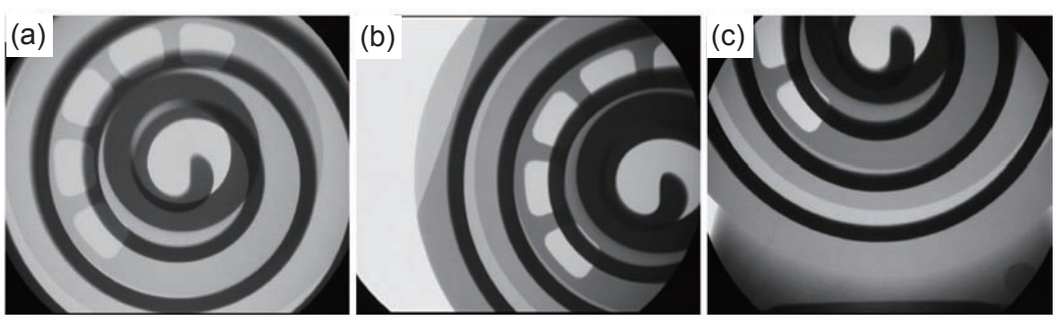

Fig. 19: X-ray detection of the central (a), left (b), and bottom (c) part of the scroll casting fabricated by SSSC process

4 Conclusions

(1) The flow velocity of the slurry significantly increases, and the area of the high-speed region enlarges with an increase in pouring temperature. The average velocity in the ingate grows linearly with an increase in the pouring temperature due to the low viscosity at a high temperature.

(2) The homogeneity of the temperature and velocity field in the slurry is improved with the increase in mold temperature. The average velocity in the ingate increases with the increase of mold temperature.

(3) The most homogeneous temperature field is obtained at the squeezing velocity of 0.5 $m \cdot s^{-1}$, while the most homogeneous velocity field is observed at the squeezing velocity of 0.3 $m \cdot s^{-1}$. Both the filling time and its variation rate decrease with the increase in the squeezing velocity.

(4) The effect of mold temperature on the temperature distribution is greater than the pouring temperature. The shrinkage area is decreased by increasing the mold temperature. The maximum solidification time shows a linear variation with the increase in pouring temperature.

(5) The recommended process parameters of the SSSC process in this work are the pouring temperature of 595 °C, the mold temperature of 350 °C, and the squeezing velocity of 0.3 $m \cdot s^{-1}$.

Acknowledgments

This work was financially supported by the China Postdoctoral Science Foundation (Grant No. 2018M 643627), the Open Foundation from the CAS Key Laboratory of Cryogenics, TIPC (Grant No. CRYO201810), the Fundamental Research Funds for the Central Universities (Grant No. XZY012019003 /XZD012019009), and the Open Foundation of the State Key Laboratory of Fluid Power and Mechatronic Systems (Grant No. GZKF-201912).

References

[1] Tello-Oquendo F M, Navarro-Peris E, Barceló-Ruescas F, et al. Semi-empirical model of scroll compressors and its extension to describe vapor-injection compressors. Model description and experimental validation. International Journal of Refrigeration, 2019, 106: 308–326.

[2] Ma X, Zhang C H, Li K. Hybrid modeling and efficiency analysis of the scroll compressor used in micro compressed air energy storage system. Applied Thermal Engineering, 2019, 161: 114–139.

[3] Iglesias A and Favrat D. Innovative isothermal oil-free co-rotating scroll compressor-expander for energy storage with first expander tests. Energy Conversion and Management, 2014, 85: 565–572.

[4] Zhang Q Q, Feng J M, Wen J, et al. 3D transient CFD modelling of a scroll-type hydrogen pump used in FCVs. International Journal of Hydrogen Energy, 2018, 43(41): 19231–19241.

[5] Jiang Z, Harrison D K and Cheng K. Computer-aided design and manufacturing of scroll compressors. Journal of Materials Processing Technology, 2003, 138(1-3): 145–151.

[6] Yoshimura H and Tanaka K. Precision forging of aluminum and steel. Journal of Materials Processing Technology, 2000, 98(2): 196–204.

[7] Shan D B, Xu W C, Lu Y. Study on precision forging technology for a complex-shaped light alloy forging. Journal of Materials Processing Technology, 2004, 151(1): 289–293.

[8] Bayramoglu M, Polat H and Geren N. Cost and performance evaluation of different surface treated dies for hot forging process. Journal of Materials Processing Technology, 2008, 205(1): 394–403.

[9] Li X, Xiong S M, Guo Z. Correlation between porosity and fracture mechanism in high pressure die casting of AM60B alloy. Journal of Materials Science & Technology, 2016, 32(1): 54–61.

[10] Zhang P, Li Z M, Liu B L, et al. Improved tensile properties of a new aluminum alloy for high pressure die casting. Materials Science and Engineering: A, 2016, 651: 376–390.

[11] Wang Y F, Zhao S D, Zhao X Z, et al. Effects of isothermal treatment parameters on the microstructure of semisolid alloys. Materials Science and Technology, 2018, 34(1): 104–110.

[12] Fu J L, Wang K K, Li X W, et al. Microstructure evolution and thixoforming behaviorof 7075 aluminum alloy in the semi-solid state prepared by RAP method. International Journal of Minerals, Metallurgy and Materials, 2016, 23(12): 1404–1415.

[13] Fu J L, Yang D, Wang K K. Correlation between the liquid fraction, microstructure and tensile behaviors of 7075 aluminum alloy processed by recrystallization and partial remelting (RAP). Metals, 2018, 8(7): 508.

[14] Jiang J F, Chen G, Wang Y. Compression mechanical behaviour of 7075 aluminium matrix composite reinforced with nano-sized SiC particles in semisolid state. Journal of Materials Science & Technology, 2016, 32(11): 1197–1203.

[15] Wannasin J, Fuchs M, Lee J Y, et al. GISS technology: principle and applications in die casting. Solid State Phenomena, 2019, 285: 470–475.

[16] Zhao Z D, Chen Q, Wang Y B, et al. Microstructural evolution of an ECAE-formed ZK60-RE magnesium alloy in the semi-solid state. Materials Science and Engineering: A, 2009, 506(1): 8–15.

[17] Balan T, Becker E, Langlois L, et al. A new route for semi-solid steel forging. CIRP Annals-Manufacturing Technology, 2017, 66(1): 297–300.

[18] Abbasi-Khazaei B and Ghaderi S. A novel process in semi-solid metal casting. Journal of Materials Science & Technology, 2012, 28(10): 946–950.

[19] Dao Vanluu, Zhao Shengdun, Lin Wenjie, et al. Effect of process parameters on microstructure and mechanical properties in AlSi9Mg connecting-rod fabricated by semi-solid squeeze casting. Materials Science and Engineering: A, 2012, 558: 95–102.

[20] Jiang J F, Wang Y, Xiao G F, et al. Comparison of microstructural evolution of 7075 aluminum alloy fabricated by SIMA and RAP. Journal of Materials Processing Technology, 2016, 238: 361–372.

[21] Lee J H, Won C W, Cho S S, et al. Effects of melt flow and temperature on the macro and microstructure of scroll compressor in direct squeeze casting. Materials Science and Engineering: A, 2000, 281(1–2): 8–16.

[22] Masoumi Mohsen and Hu Henry. Influence of applied pressure on microstructure and tensile properties of squeeze cast magnesium Mg-Al-Ca alloy. Materials Science and Engineering: A, 2011, 528(10–11): 3589–3593.

[23] Ma Z, Zhang H R, Song W, et al. Pressure-driven mold filling model of aluminum alloy melt/semi-solid slurry based on rheological behavior. Journal of Materials Science & Technology, 2020, 39: 14–21.

[24] Zhang Y, Wu G H, Liu W C, et al. Microstructure and mechanical properties of rheo-squeeze casting AZ91-Ca magnesium alloy prepared by gas bubbling process. Materials & Design, 2015, 67: 1–8.

[25] Atkinson H V. Modelling the semisolid processing of metallic alloys. Progress in Materials Science, 2005, 50(3): 341–412.

[26] Fu J L, Wang K K. Modelling and simulation of die casting process for A356 semi-solid alloy. Procedia Engineering, 2014, 81: 1565–1570.

[27] Jahajeeah N. Application of numerical modelling in SSM automotive brake calliper castings. Journal for New Generation Sciences, 2006, 4: 94–99.